I&EC research
Industrial & Engineering Chemistry Research

Article

Cite This: Ind. Eng. Chem. Res. 2019, 58, 7296−7307

pubs.acs.org/IECR

Batch and Continuous Systems for Zn, Cu, and Pb Metal Ions Adsorption on Spent Mushroom Compost Biochar

Maha M. Abdallah,[†,‡] Mohammad N. Ahmad,[‡] Gavin Walker,[†] James J. Leahy,[†] and Witold Kwapinski*,[†]

[†]Department of Chemical Sciences, Faculty of Science and Engineering, Bernal Institute, University of Limerick, Limerick V94 T9PX, Ireland

[‡]Department of Chemical and Petroleum Engineering, American University of Beirut, Beirut 1107 2020, Lebanon

ABSTRACT: Spent mushroom compost biochar (SMCB) was prepared by carbonization and tested for the removal of heavy metals (Zn(II), Cu(II), and Pb(II)) by adsorption. The sorption of heavy metals was evaluated by studying several factors, such as the initial solution pH, contact time, temperature, and individual and competitive adsorption. Kinetic and equilibrium studies were carried out to determine the mechanism involved during adsorption. The Weber−Morris model demonstrated the significance of intraparticle diffusion on the adsorption process. In addition, thermodynamic studies showed that the process is endothermic and favorable, with good affinity of metals to the biochar. At last, SMCB was used as the adsorbent in a continuous fixed-bed column. The breakthrough curve was obtained for each heavy metal, and Thomas and Clark models were fitted. When all three metals coexisted in solution, competitive adsorption took place in both batch and continuous systems, showing that Pb has higher affinity to SMCB than Cu and Zn.

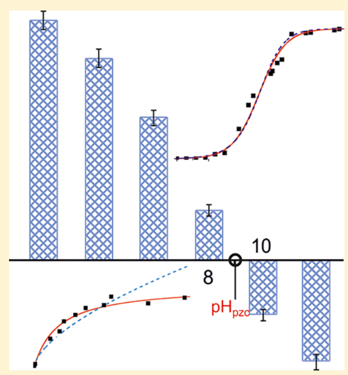

1. INTRODUCTION

Highly hazardous contaminants, such as heavy metals, are generated by industrial processes and discharged in wastewater and the natural ecosystem without adequate treatment.[1] Heavy metals present in the wastewater can be absorbed by plants and thus affect humans and living organisms.[2] They include lead, cadmium, zinc, copper, mercury, nickel, arsenic, and several others. Their accumulation in the soil and vegetation system is highly toxic, as they can be consumed by micro-organisms and become incorporated in the food chain.[3]

The use of biochar, a nontoxic byproduct generated from agricultural wastes,[4] can replace some more expensive adsorbents used for the removal of heavy metals from wastewater. Biochar is a product formed during the carbonization of biomass by pyrolysis.[5,6] Its properties are similar to those of charcoal as it contains a high amount of organic carbon and includes aromatic structures that enhance the adsorption capacity of the biochar.[7] Biochar has a lower surface area and porosity compared to activated carbon, however, it has a higher content of oxygen-containing acid groups that increase the metal sorption efficiency.[8] The pore size, molecular structure, and characteristics of the biochar depend on the biomass used and the carbonization conditions during its preparation.[9] Therefore, in this study, spent mushroom compost is investigated as a potential biomass to prepare biochar for an effective and adequate treatment of wastewater by adsorption. The application of this biomass is highly important due to its significantly increasing waste production, which emphasizes the need for its adequate management in a green wastewater treatment.

Spent mushroom compost is the residual waste obtained after the mushroom crop has been harvested. One kilogram of mushrooms can result in approximately 5 kg of spent mushroom compost.[10] More than 3.5×10^6 tons of spent mushroom compost are generated annually in the European Union, and an estimate of 295000 tons is produced yearly by the Irish mushroom industry.[11,12] Spent mushroom compost contains a high amount of organic nutrients as it is produced from wheaten straw, poultry manure, gypsum mixed with cottonseed, and mushroom waste. Therefore, their composition, high abundance, and low cost have attracted much attention for their application as biomass for the production of biochar.[13] In previous studies, the conversion of this biomass to biochar has been shown to be a potential amendment of soil to increase the quality of the biofertilizers.[13] Biochar was significantly used in soil amendment due to its ability to sequester carbon and adsorb various potentially toxic elements on its surface.[14] Its addition to compost enhances the microbial activity and significantly increases the organic matter and nutrients such as N, K, and P in the compost material. In fact, it has been proven that mixing biochar with compost reduced the mobility of Pb and Cu in soil, which induced seed germination and root elongation in soil.[15,16]

Sorbents prepared from agricultural or industrial byproducts are reported to be promising materials for removal of metal ions from aqueous solution.[17] In a previous study, spent mushroom compost biochar (SMCB) was used as a potentially efficient

Received: February 6, 2019
Revised: March 29, 2019
Accepted: April 15, 2019
Published: April 15, 2019

biosorbent to remove fluorine from water.[10] The removal of organic pollutants can involve different possible mechanisms, such as ion exchange, metal binding, redox reaction, surface adsorption, and precipitation.[18] Hence, during carbonization, biochar forms a large number of functional groups which induce its polarizability and the remediation of heavy metal ions.[18,19]

The majority of studies are limited to batch adsorption; however, it is very important to perform continuous adsorption to obtain accurate scale-up data for engineers to be able to design a large, industrial-scale process.[20] In this study, the use of SMCB has been investigated for the adsorption of heavy metals: zinc (Zn(II)), copper (Cu(II)), and lead (Pb(II)). The effect of initial solution pH, adsorption kinetic at various temperature, and the sorption isotherms of Zn^{2+}, Cu^{2+}, and Pb^{2+} were investigated to establish the adsorption mechanism onto SMCB. Fixed-bed continuous adsorption was used to study the dynamic behavior in the column, which can be represented by breakthrough curves (BTC).[21] Mathematical models were applied to analyze the BTC of the metals to be removed. As water treatment includes the simultaneous removal of several metals, the role of competitive adsorption is essential. The adsorption capacity of the heavy metals changes when they coexist in the same medium. The competitive adsorption is mainly controlled by the forces of ion exchange and functional group binding, and it is affected by the concentration of the metal cations present. It has been shown that intense competitive adsorption takes place when the competitor ion concentration increases due to the heterogeneous distribution of the binding forces on the biochar adsorption sites.[14,22] Consequently, this study investigates the co-occurrence of three metals at various initial concentrations using both batch and continuous adsorption techniques.

2. MATERIALS AND METHODS

2.1. Materials Used. Locally available spent mushroom compost was used in this study. The material was dried at 100 °C for 24 h and then carbonized at a temperature of 500 °C for 3 h under oxygen-limited conditions using a Lenton furnace (laboratory chamber furnace). The SMCB was then ground (using a grinder) and sieved to obtain fine particle size between 0.180 and 0.425 mm.

Stock solutions of $CuCl_2$ (>98% Merck part no. 8.18247.0500), $ZnCl_2$ (98% Aldrich part no. 20.808-6), and $Pb(NO_3)_2$ (99.5% Riedel de Haen part no. 11520) were prepared, using deionized water, as sources of the metal ions Cu(II), Zn(II), and Pb(II) at a concentration of 3×10^{-3} mol/L.

2.2. Characterization of SMCB. The total amount of C, H, and N was analyzed using an elemental analyzer (Elemental Vareo el Cube Analyzer). The moisture content of spent mushroom compost was obtained according to the standard. Solid recovered fuels: Determination of moisture content using the oven drying method ICS 75.160.10, DD CEN/TS 15414-1:2010. The ash content for spent mushroom compost and SMCB was determined according to ICS 75.160.10, EN 14775:2009. The volatile matter was determined according to ICS 75.160.10, EN 15402:2011. The higher heating value was obtained using a Parr 6200 calorimeter. The Brunauer–Emmet–Teller surface area of the biochar was determined using multipoint method (Autosorb-1, Quantachrome Instruments, USA). Before analysis, samples were vacuum degassed at 200 °C for 4–16 h. The degassing time varied on the basis of the time necessary to reach a stable surface area measurement.

The surface functionality of the biochar surface before and after adsorption was investigated using Fourier transform infrared (FTIR) spectroscopy (Cary 630 FTIR with MicroLab Software) to assess if the adsorption mechanism involves modifications and chemical interactions on the surface functional groups of SMCB. The biochar samples were further finely ground and analyzed at 8 cm^{-1} resolution for a total of 32 sample scans in the wavenumber range of 4000–650 cm^{-1}.

The cation-exchange capacity (CEC) of SMCB was estimated using an NH_4^+ replacement method[23] to assess the involvement of ion exchange during the adsorption process. It was determined by the replacement of the Na^+ ions with NH_4^+ ions. One gram of SMCB was added to a sodium acetate solution (20 mL, 1.0M) to saturate the exchange sites. The solution was then transferred to an extraction column containing cotton wool where it was leached using the same sodium acetate solution and then four times with ethanol (30 mL, 98%) until the conductivity of the extract was less than 40 $\mu S \cdot cm^{-1}$ to remove excess sodium acetate. The conductivity was measured using a Jenway 4510 conductivity meter. In order to replace the adsorbed Na^+ ions, leaching with ammonium acetate (30 mL, 1.0 M) was repeated three times. The extract was then analyzed using a Varian Spectra AA220 atomic absorption spectrophotometer (AAS) at a wavelength of 330.3 nm to determine the Na^+ content and calculate the CEC.[24]

2.3. Effect of Initial pH. The 50 mL samples of metals solutions (3×10^{-3} mol/L) were prepared, and the pH of the solution was corrected to pH 6 using sodium hydroxide Na(OH) and nitric acid HNO_3 (AnalaR NORMAPUR) before the biochar was added. The samples were shaken with 0.5 g of SMCB using an IKA WERKE RT 15 power at a constant speed of 240 rpm using a magnetic stirrer for specific periods of time, based on the experiments conducted. The experiments were conducted using the batch technique by adjusting the initial solution pH to 2, 4, 6, 8, 10, and 12. At equilibrium, the pH of the solution was measured to assess the change in pH.

The pH of the solutions was adjusted to a value 6 after adsorption to ensure that precipitation of the heavy metals does not affect the adsorption process. The pH adjustment before filtration ensures that the removal of any precipitated heavy metals by filtration is avoided prior to analysis. Triplicate samples were taken with a 5 mL syringe (Omnilab-Laborzentrum GmbH) and filtered through a 0.450 μm membrane filter (Filtropur S 0.45) and the concentration of the remaining metal ions was analyzed using AAS at a wavelength of 327.4 nm for Cu, 283.3 nm for Pb and 213.9 nm for Zn.

The adsorption capacity at time t, q_t (mg/g), was obtained according to eq 1

$$q_t = \frac{(C_0 - C_t)V}{m} \quad (1)$$

where C_0 is the initial concentration of metal ion (mg/L), C_t is the concentration remaining of the metal ion (mg/L), V is the volume of the sample (L), and m is the mass of the biochar in the sample (mg). The adsorption capacity q_e was calculated using eq 1 with C_t as the concentration of metal ion obtained at equilibrium (mg/L).

The point of zero charge (pH_{pzc}) was obtained for the adsorption using SMCB. It was assessed graphically by plotting the initial pH (pH_{in}) as a function of ΔpH given by eq 2. The pH_{pzc} was taken as the value where $\Delta pH = 0$.[25]

DOI: 10.1021/acs.iecr.9b00749
Ind. Eng. Chem. Res. 2019, 58, 7296–7307

$$\Delta pH = pH_e - pH_{in} \quad (2)$$

2.4. Adsorption Isotherms. The adsorption capacity of metal cations on the biochar can be analyzed using equilibrium isotherms. The most common models used for metal sorption are the Langmuir and Freundlich models. The Langmuir model assumes a monolayer adsorption onto the homogeneous and energetically equivalent surface containing the adsorption sites, where once they are filled, no additional sorption can take place on this site. Therefore, the surface achieves a maximum adsorption when the saturation point is reached. This isotherm is represented by eq 3

$$q_e = \frac{q_0 K_L C_e}{1 + K_L C_e} \quad (3)$$

where C_e is the equilibrium concentration (mg/L), q_e is the amount adsorbed at equilibrium (mg/g), q_o (mg/g) is the maximum sorption capacity, and K_L (L/mg) is the constants characteristic of the Langmuir equation. They can be obtained by plotting the specific adsorption (C_e/q_e) as a function of C_e.

The Freundlich model is an empirical model that represents a multilayer adsorption onto a heterogeneous surface with varying affinities. The binding sites with a stronger affinity are occupied first and the energy of the sorption sites decreases with increasing site occupation until the adsorption process is completed. Equation 4 represents this sorption isotherm

$$q_e = K_f C_e^{1/n} \quad (4)$$

where n is a Freundlich constant and K_f is a temperature-dependent constant. They can be obtained by plotting $\ln(q_e)$ as a function of $\ln(C_e)$.[26]

The separation factor R_L is determined to study the shape of the isotherm: unfavorable when $R_L > 1$, linear when $R_L = 1$, favorable when $0 < R_L < 1$ and irreversible when $R_L = 0$[21]

$$R_L = \frac{1}{1 + bC_0} \quad (5)$$

where b is the Langmuir constant and C_0 is the initial concentration of the adsorbate (mg/L).

2.5. Adsorption Kinetics. The kinetic models investigated in this study are pseudo-first order (PFO), pseudo-second order (PSO), and Weber–Morris (WM) models. The PFO model describes the rate of the liquid–solid phase adsorption system based on eq 6[27]

$$\log(q_e - q_t) = \log(q_e) - \frac{k_1 t}{2.303} \quad (6)$$

where q_e and q_t represent the adsorption capacity (mg/g) at equilibrium and time t (min), respectively, and k_1 is the first-order rate constant (min^{-1}).

Another kinetic model is based on the PSO rate law, described by eq 7:

$$\frac{t}{q_t} = \frac{t}{q_e} + \frac{1}{h} \quad (7)$$

The amount of sorbate per adsorbent mass and time, h, can be obtained using eq 8, where k_2 is the PSO rate constant (g·mg^{-1}·min^{-1}).[28] It can be used to compare the sorption rate of the cations on SMCB at different sorption process temperatures.

$$h = k_2 q_e^2 \quad (8)$$

The WB model was developed to investigate if the internal resistance is the limiting step, based on eq 9[29]

$$q_t = k_i t^{1/2} + \beta \quad (9)$$

where k_i is the intraparticle WB rate constant (mg·g^{-1}·min$^{-1/2}$) and β describes the thickness at the boundary layer during adsorption.

2.6. Thermodynamics Test. The effect of temperature on the adsorption process was investigated by varying the temperature of the sample solutions: 20, 40, and 60 °C. The samples were heated then the biochar was added (0.5 g), and the solution was stirred overnight to ensure that equilibrium is reached. Thermodynamic parameters were obtained usingeqs 10–12)[30,31]

$$\Delta G° = \Delta H° - T\Delta S° \quad (10)$$

$$\Delta G° = -RT \ln(K_e) \quad (11)$$

$$\ln(K_e) = \frac{\Delta S°}{2} - \frac{\Delta H°}{RT} \quad (12)$$

where $\Delta G°$ is the Gibbs free energy change, $\Delta H°$ is the enthalpy change (kJ/mol), and $\Delta S°$ is the entropy change (kJ/mol). R is the gas constant (8.314 J mol^{-1}K^{-1}), and T is the temperature of the adsorption process (K). K_e is the thermodynamic equilibrium constant, also defined as the distribution coefficient, and can be determined using eq 13

$$K_e = \frac{C_a}{C_e} \quad (13)$$

where C_a is the equilibrium concentration of the adsorbate on the adsorbent (mg/L) and C_e is the equilibrium concentration of the adsorbate in solution (mg/L).[32]

2.7. Continuous Adsorption. *2.7.1. Fixed-Bed Column Design.* A laboratory-scale column was used to perform the adsorption of the heavy metals in a continuous system. Metal ion solutions were prepared at a concentration of 3×10^{-3} mol/L using $Zn(Cl)_2$, $Cu(Cl)_2$, and $Pb(NO_3)_2$. The same concentration was prepared when a mixture of the three metals ions is used. A layer of 2 cm in height of glass spheres (1 mm diameter) was set at the top and bottom of the column (2.5 cm high and inner column diameter 1.9 cm) to ensure good stacking of the adsorbent and to avoid channeling of influent solution during the adsorption process. At the bottom of the bed between the glass spheres bottom layer and the adsorbent layer, glass wool was used to ensure a proper separation between the two layers and to avoid having the biochar washed away with the solution during the experiments.[33]

The influent solution was pumped into the column at a flow rate of 1.6 mL/min using a peristaltic pump (Ismatec Ecoline VC-MS/CA8-6). At first, the column is primed with distilled water to remove any excess air. Then the sorbate solution is passed into the column and the samples of the effluent solution are collected at specific periods of time. The samples are taken to the AAS to obtain the amount of each metal ions.

2.7.2. Fixed-Bed Column Adsorption Modeling. The breakthrough curve is obtained using experimental data by plotting C_{out}/C_{in} as a function of time. Mathematical models were applied to analyze the breakthrough behavior in the fixed-bed adsorber.

2.7.2.1. Thomas Model. The Thomas model states that adsorption is immediate. It is based on the assumption that the adsorption undergoes pseudo-second-order kinetics, and that

DOI: 10.1021/acs.iecr.9b00749
Ind. Eng. Chem. Res. 2019, 58, 7296–7307

electrostatic interactions and axial dispersion are negligible.[34] It is described by eq 14

$$\ln\left(\frac{C_{in}}{C_{out}} - 1\right) = -k_T C_{in} t + \frac{k_T q_{max} m}{\nu} \tag{14}$$

where k_T is the Thomas rate constant (L/(min·mg)), q_{max} is the maximum adsorption concentration in the solid phase (mg/L), m is the mass of adsorbent used, and ν is the volumetric flow rate (L/min).

2.7.2.2. Clark Model. The Clark model was developed to study the performance of adsorption using the eq 15[35]

$$\ln\left[\left(\frac{C_{in}}{C_{out}}\right)^{n-1} - 1\right] = -rt + \ln B \tag{15}$$

where n is the Freundlich constant and r and B are the Clark model parameters. This model assumes that the Freundlich isotherm applies and that the adsorption rate is limited by the outer mass transfer step.

3. RESULTS AND DISCUSSION

3.1. Characterization of SMCB. The properties of SMCB and proximate analysis of noncarbonized spent mushroom compost and SMCB are presented in Table 1. The SMCB

Table 1. Selected Properties of Spent Mushroom Compost (Raw and Carbonized Material)

parameters[a]	spent mushroom compost	SMCB
moisture content, wt %	45.8	
ash content, wt $\%_{db}$	16.4	50.6
volatile matter, wt $\%_{db}$	71.4	13.8
fixed carbon, wt $\%_{db}$	8.9	35.6
C, wt $\%_{db}$		35.94
H, wt $\%_{db}$		1.21
N, wt $\%_{db}$		2.18
O, wt $\%_{db}$*		38.83
surface area, $m^2 \cdot g^{-1}$		9.2
higher heating value, $MJ \cdot kg^{-1}$		13.8
CEC, $mmol \cdot kg^{-1}$		57.6
pH		8.8

[a]db: calculated on a dry basis. *: calculated by difference.

surface area is 9.2 m^2/g. The moisture content of the raw material before carbonization was relatively high (45.8 wt %) as for the majority of biowastes. The fixed carbon increased after carbonization from 8.9 wt % to 21.2 wt % (calculated on a dry basis) and is relatively low due to the high ash content that increased from 16.4 to 50.6 wt %. However, the volatile matter in spent mushroom compost decreased significantly from 71.4 to 13.8 wt %. The relatively high amount of ash content (50.6 wt %) of SMCB indicates the presence of a large fraction of mineral parts. The higher heating value (HHV) for SMCB is 13.8 MJ/kg. It has been shown in previous studies that the HHV of biochar range from 12 to 44 MJ/kg, while the heating value of coal and charcoal is the range of 14 to 35 MJ/kg.[36] Carbonisation is an important process during which energy densification takes place: low-energy components are volatized and high-energy components remain within the product obtained[37] suggesting that biochar is a potential material for replacement of solid fossil fuels for cleaner energy production.

The surface functional groups were analyzed using FTIR, as presented in Figure 1. The SMCB showed three strong peaks:

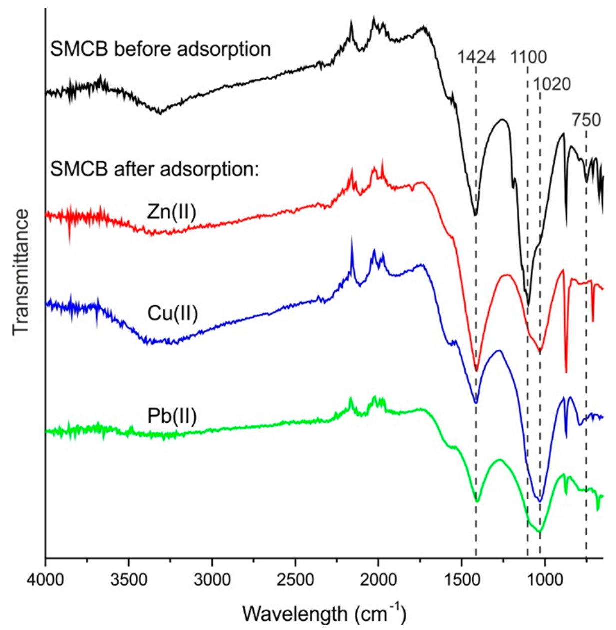

Figure 1. FTIR spectra of SMCB before and after adsorption of Zn, Cu, and Pb ions.

one at 1100 cm^{-1} corresponding to an aliphatic ether C−O stretching vibration and the other peaks at 1424 and 877 cm^{-1} indicating the presence of the carbonate stretching and bending vibrations respectively of carbonate.[38] In addition, peaks at 1566 and 1722 cm^{-1} indicate stretching vibrations of nitro N−O and aliphatic C═O, respectively.[39] The chemical interactions between the biochar and its environment are related to the surface chemistry of the biochar. Thus, the presence of oxygenated functional groups suggests that adsorption may involve interactions with the functional groups present on the surface of SMCB. For the adsorption of the metal ions, the peak at 750 cm^{-1} visible on SMCB before adsorption is less visible after the sorption. This is because most of the binding sites were used by metal ions for coordination. As the C−H stretching was affected, the M−C bond could be a metal−methylidyne (MCH), metal−methylidene (MCH_2), or methyl−metal (MCH_3) bond depending upon the ligand attached to the carbon atom.[40] After adsorption, the peak at 1100 cm^{-1} underwent a shift to lower wavenumber (1020 cm^{-1}) due to adsorption of the metal and weakening of the C−O bond.[41] At 3300 cm^{-1} in case of Pb(II) adsorption, the O−H alcohol peak disappeared after the Pb(II) adsorption, which was later shown to be a higher sorption effect, demonstrating that chemical interactions took place between the heavy metal cations and the surface functional groups of SMCB during adsorption.

The cation-exchange capacity (CEC) is the total amount of exchangeable cation (such as Na^+, Ca^{2+}, K^+, Fe^{2+}, NH_4^+, Mg^{2+}, etc.) associated with sites on the biochar. Biochar has a specific metal-binding capacity mainly due to the presence of hydroxyl, phenolic, carboxylate, and carbonyl groups. Therefore, biochar that contains more hydrophilic and oxygen groups possesses higher cation-exchanging ability and a higher nutrient retention capacity.[42] The CEC study was undertaken to investigate the involvement of the ion-exchange mechanism in the adsorption process of the metal ions onto SMCB. It was found to be

DOI: 10.1021/acs.iecr.9b00749
Ind. Eng. Chem. Res. 2019, 58, 7296−7307

moderate with a value of 57.6 mmol/kg. Biochar prepared from poultry litter and swine manure has the CEC of 70.3 and 91.4 mmol/kg, respectively, when carbonized at 400 °C but it falls to 39.7 and 36.3 mmol/kg, respectively, when carbonized at 600 °C.[43] The results show that at higher pyrolysis temperature, the CEC decreases, proving that the ion exchange process becomes less important at higher temperatures.

The adsorption is highly affected by the chemical groups present on the biochar surface. After carbonization, the surface area of the biochar is modified and many functional groups are formed on the surface. At low carbonization temperature, the oxygenated functional groups, such as carboxylic and phenolic, are not decomposed. These groups can induce a greater nutrient retention capacity and a higher cation exchange. When increasing the temperature, the C/O ratio increases and more aromatic compounds are formed. In this case, adsorption occurs mainly by electrostatic (cation−π) interaction and it is known as physisorption.[44−46]

3.2. Effect of Initial pH. The initial pH of the solution plays a significant role in the adsorption process as it affects the surface charge of the adsorbent and the degree of precipitation of the metal ions in the solution. Figures 2 shows that ΔpH decreases

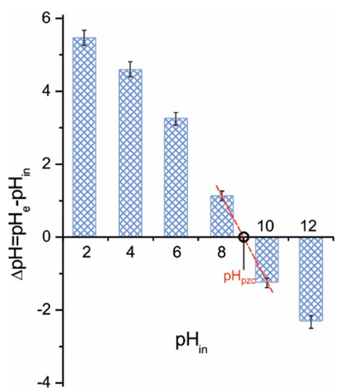

Figure 2. pH changes during Pb ions adsorption on SMCB (pH_{in} and pH_e are the initial solution pH and the pH at equilibrium, respectively).

with increasing initial pH value for Pb(II) ion adsorption on SMCB. At low pH values, the biochar surface is protonated and more positively charged and, thus, decreases the adsorption capacity of the positively charged metal ions. During an adsorption, at low initial pH values, the pH increased significantly (from 2 to 6.1 for Zn(II), 6.2 for Cu(II), and 7.5 for Pb(II)), which shows that precipitation took place. The increase in pH is likely associated with the dissolution of mineral solids that exist in SMCB, as the characterization of SMCB showed that it contains a large fraction of ash (50.6% ash). The lower the initial pH, the higher the destabilizing conditions imposed on the existing solids in the biochar ash. As the pH increases, deprotonation takes place, which liberates more binding sites and leads to increased adsorption. The increase in pH leads to complex ion formation ($MeOH^+$), which increases the sorption of the cations onto SMCB.[47] The point of zero charge (pH_{pzc}) is the pH value at which the total charge of the internal and external surface of the biochar is zero. It is an important factor for the surface characterization of the sorbent.[48] This shows that basic and oxygenated functional groups are dominant on the biochar surface. In the case of SMCB material, the pH_{pzc} is close to 9.0. The pH_{pzc} is a property of a material, and it is irrespective of the sorbate, than the results are presented for Pb ions only in Figure 2. It has been shown in the literature[49] that the pH_{pzc} value of biochar depends on carbonization temperature and conditions and is in the region confirmed by this work.

As shown in Figure 3, the optimum pH for the sorption of the heavy metals is 6, the value at which further experiments were

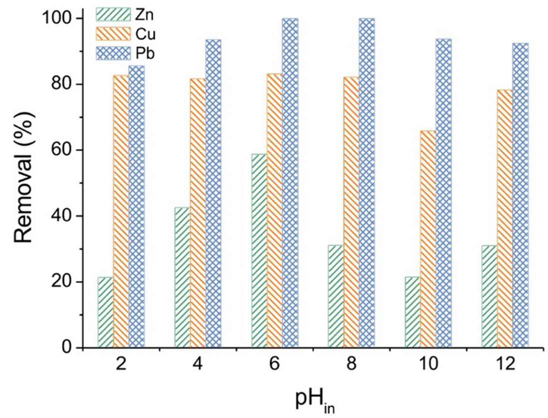

Figure 3. Percent of ions removal as a function of initial pH. (pH_{in} is the initial solution pH).

conducted. At equilibrium, the pH value of 6 increased to 8.20, 8.18, and 9.26 for the removal of Zn(II), Cu(II), and Pb(II), respectively. Thus, the mineral part of the biochar plays a major role in the increase of the solution pH leading to precipitation. At higher pH values, the ionic charge of the surface is decreased by hydrolysis and the precipitation of the metals $Me(OH)_2$ occurs, which lowers the interaction between the cations in the solution and the surface of the biochar. The adjustment of the pH of the solutions to a value of 6 was done to avoid the influence of precipitation on the adsorption process. The influence of initial pH of the solution was investigated in different studies to assess its effect on the sorption process. In a previous study,[50] precipitation is found to occur at a pH of 7.75 and higher, the cation in solution precipitates to form metal hydroxide which decreased the adsorption capacity. These results conform with another study[51] in which at higher pH values, the dominant species were $Me(OH)_2$ which decreased the adsorption. The highest removal took place at a pH of 5, at which ($MeOH^+$) species were dominant. Thus, the pH affects the adsorption as the surface charge which increases or reduces the electrostatic interactions as well as ion exchange and deposition.

3.3. Adsorption Isotherms. The adsorption equilibrium and its empirical models are significant for the application of biochar as adsorbents. They provide the basis to further understand an interaction between an adsorbent and an adsorbate, which is affected by the properties of the adsorbent used.[26] The adsorption data of the metal ions on SMBC samples were analyzed using the Langmuir and Freundlich isotherm models. Parts a−c of Figure 4 present the isotherms along with the experimental data. As presented in Table 2, the best fitting model for the adsorption of Zn and Pb ions is the Langmuir isotherm (based on R^2 values), showing that a monolayer adsorption may be formed during adsorption over energetically equivalent adsorption sites. The values of R_L are in the range of 0.004−0.190, implying that the adsorption process may be favorable. As for the Cu ion, the best fit model is Freundlich with a higher R^2 value than Langmuir. Thus, adsorption for this metal

DOI: 10.1021/acs.iecr.9b00749
Ind. Eng. Chem. Res. 2019, 58, 7296−7307

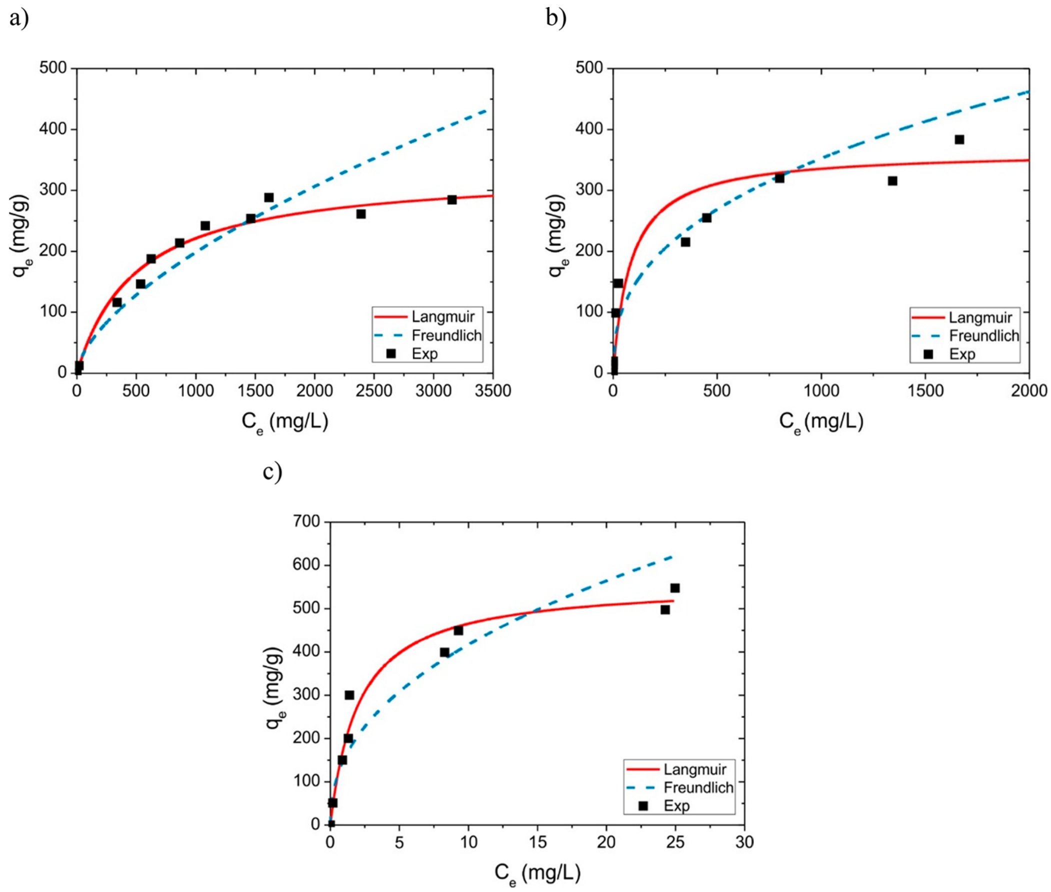

Figure 4. Adsorption isotherms of (a) Zn, (b) Cu, and (c) Pb on SMCB.

Table 2. Langmuir and Freundlich Isotherm Parameters for the Adsorption of Heavy Metal Ions

		Langmuir				Freundlich		
metal ion	$q_{e,\,exp}$, mg·g^{-1}	q_0, mg·g^{-1}	K_L, L·mg^{-1}	R_L	R^2	K_F, mg·g^{-1}	n	R^2
Zn(II)	288.5	333.2	0.002	0.602	0.964	2.61	1.595	0.806
Cu(II)	383.5	364.2	0.012	0.190	0.912	23.75	2.561	0.950
Pb(II)	547.5	564.0	0.455	0.004	0.957	158.10	2.339	0.899

Table 3. Kinetics Parameters for the Adsorption of Heavy Metals Using SMCB

			pseudo-first-order model			pseudo-second-order model				Weber−Morris model		
metal ion	T, °C	$q_{e,\,exp}$, mg·g^{-1}	q_1, mg·g^{-1}	k_1, L·min^{-1}	R^2	q_2, mg·g^{-1}	k_2, g·mg^{-1}·min^{-1}	h, mg·g^{-1}·min^{-1}	R^2	k_i, mg·g^{-1}·min$^{-0.5}$	β	R^2
Zn(II)	20	9.65	9.72	0.013	0.950	10.08	0.003	0.29	0.969	0.701	0.22	0.971
	40	13.9	14.00	0.011	0.939	14.01	0.002	0.40	0.970	1.138	−0.56	0.919
	60	14.7	16.30	0.050	0.967	14.93	0.016	3.57	0.962	2.138	1.25	0.711
Cu(II)	20	14.83	14.84	0.184	0.939	15.09	0.021	4.86	0.972	2.722	2.32	0.984
	40	15.10	15.08	0.462	0.883	15.56	0.027	6.60	0.978	3.070	2.62	0.992
	60	15.21	15.22	0.607	0.941	15.75	0.051	12.58	0.987	3.589	2.10	0.979
Pb(II)	20	58.89	58.65	0.613	0.602	58.86	0.576	1997	0.999			
	40	59.03	58.94	0.158	0.336	58.91	1.699	5896	0.999			
	60	59.62	59.02	0.137	0.315	59.01	0.932	3245	0.999			

ion is likely to take place on a heterogeneous multilayer adsorption surface. The maximum adsorption (q_0) is higher for Pb(II) (564 mg/g) than Cu(II) (364.2 mg/g) than Zn(II) (333.2 mg/g). Compared to some other biomass origin char materials, SMCB shows good adsorption capacity. The maximum adsorption capacity for Pb removal was shown to be 22.85, 39.37, and 76.6 mg/g using different biochar derived from apricot stone,[52] soybean hulls,[53] and pecan shells,[54] respectively. Agoubordea and Navia used sawdust and brine sediment derived biochar[55] for the removal of zinc (2.58 and 4.85 mg/g, respectively) and copper (2.31 and 4.69 mg/g, respectively). The use of biochar derived from carrot residues was also investigated and treated with HCl.[56] The maximum adsorption capacity was shown to be 45, 30, and 33 mg/g for Cr,

DOI: 10.1021/acs.iecr.9b00749
Ind. Eng. Chem. Res. 2019, 58, 7296−7307

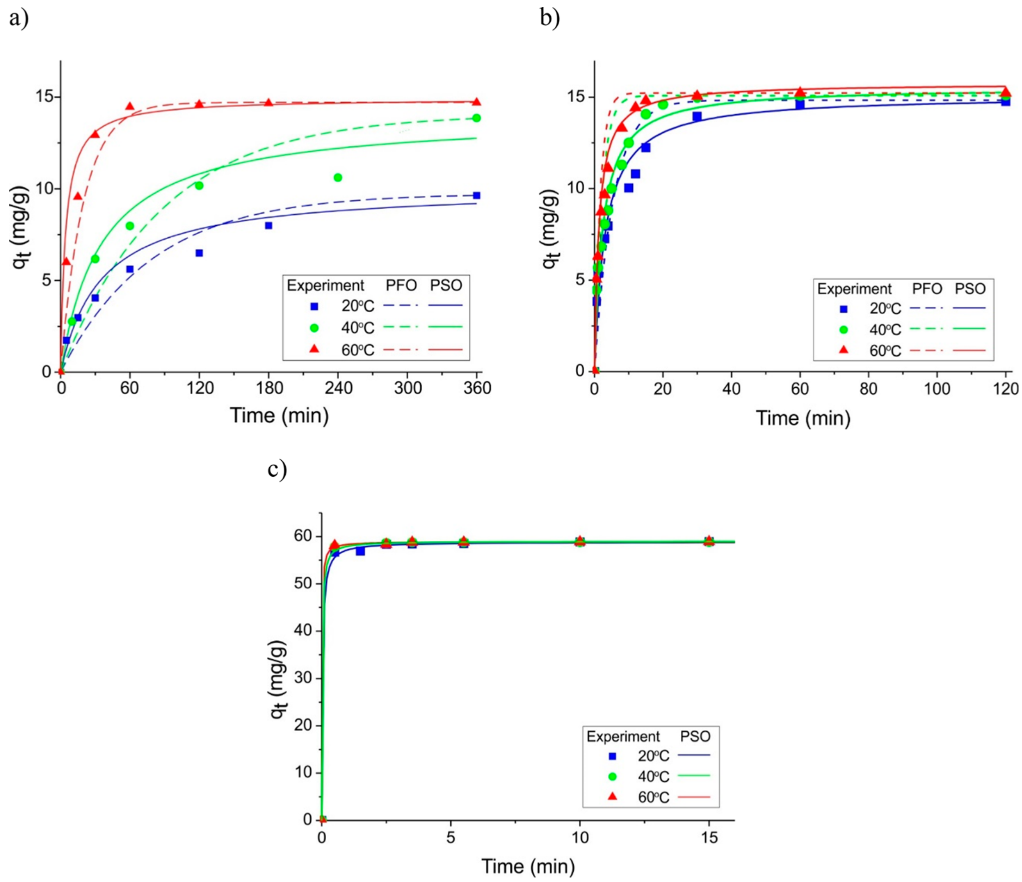

Figure 5. Kinetics for heavy metals ions (a) Zn, (b) Cu, and (c) Pb adsorption on SMCB at various temperatures. Experimental data described as pseudo-first order (PFO) and pseudo-second order (PSO).

Zn, and Cu removal, respectively. In addition, sesame straw biochar was studied, and the maximum adsorption capacity was 102, 86, 65, 55, and 34 mg/g for the removal of Pb, Cd, Cr, Cu, and Zn, respectively.[57] Thus, in comparison to application of different lignocellulosic origin biochar, the results obtained for the adsorption capacity of the heavy metals show that spent mushroom compost is a potential material for wastewater treatment.

3.4. Adsorption Kinetics. The rate of adsorption and its dynamic behavior are important factors that must be investigated for the application of biochar to wastewater treatment. Biochar prepared from different feedstocks and at different carbonization conditions possess different structure and characteristics. The adsorption rate and capacity are a function of the properties of the biochar used, such as the aromaticity, porosity, surface area, polarity, etc.[17] Determination of the kinetic parameters can help assess the rate-limiting step and the contact time required for the adsorption process in adsorbents. Three of the most frequently used models were used to assess the rate-limiting step of adsorption: PFO, PSO, and WM models. The resulting kinetic parameters are shown in Table 3 with the best fitting model having the highest correlation factor (R^2) between experimental and model data.

Parts a−c of Figure 5 display the experimental data with PFO- and PSO-fitted models for the heavy metal adsorption onto SMCB at three different temperatures. The plots show a rapid increase in the adsorption capacity at the initial stage of adsorption, followed by a plateau which signals the onset of equilibrium. At the start of the adsorption process, a higher adsorption rate is observed due to more available adsorption sites. As adsorption proceeds, a lower increase in adsorption capacity is observed due to fewer available adsorption sites, until equilibrium is reached. Figure 5a shows that as the temperature is increased from 20 to 60 °C, a significant increase in the adsorption capacity of Zn(II) is observed. The R^2 values are higher for PSO than PFO for every metal ions investigated, implying that chemisorption may be involved. For Cu(II) and Pb(II), parts b and c of Figure 5 show a less significant increase in the adsorption capacity than for Zn(II) as the temperature is increased for the other two ions. The R^2 values obtained for Cu(II) are similar for PFO and PSO models. In addition, the values of h were shown to be higher for Pb(II) than Cu(II) than Zn(II). This shows a higher driving force between SMCB and Pb(II) during the process. The adsorption capacity q_2 obtained from PSO increased from 10.08 to 14.93 mg/g for Zn(II), 14.74 to 15.75 mg/g for Cu(II), and 58.86 to 59.01 mg/g for Pb(II) when the temperature was increased from 20 to 60 °C. Thus, higher temperatures of adsorption lead to a higher heavy metal removal from the aqueous solutions. For Pb(II) ion adsorption, the R^2 values for the PFO model are very poor as the process was very fast, and determination of adsorption capacity not close to equilibrium was not possible. In this case after even a short time (few seconds) the adsorbent was almost saturated by Pb(II) ions, and kinetic constants should be determined earlier than saturation.

The WB model was studied to assess if intraparticle diffusion is the rate limiting step during the overall adsorption process. The parameters of the WM models are shown in Table 3. The

DOI: 10.1021/acs.iecr.9b00749
Ind. Eng. Chem. Res. 2019, 58, 7296−7307

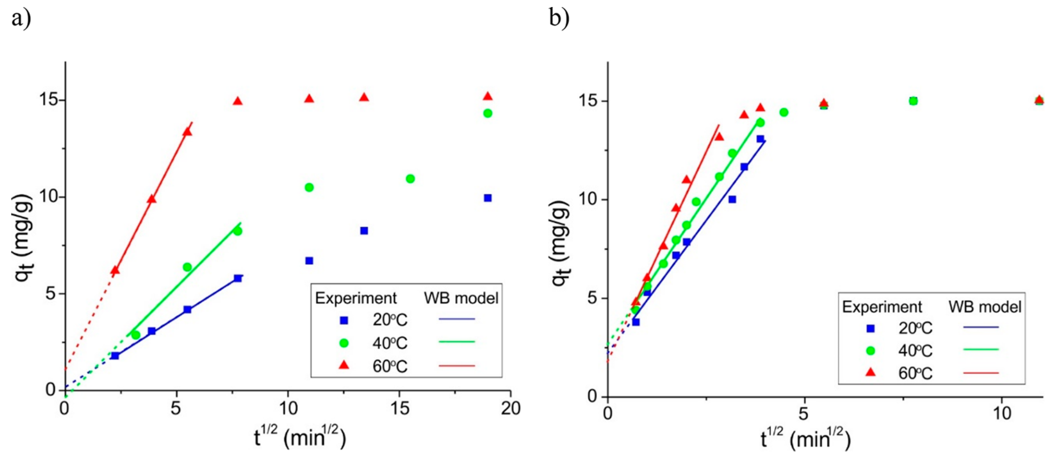

Figure 6. Kinetics for heavy metals ions (a) Zn and (b) Cu adsorption on SMCB at various temperatures. Experimental data described by intraparticle diffusion Weber−Morris (WM) model.

constant β accounts for the boundary layer thickness during adsorption. The lower this value is, the lower the boundary effect may be. A β value of zero implies that intraparticle diffusion could be the rate-limiting step. For Cu(II) and Zn(II), parts a and b of Figure 6 were plotted to show the adsorption capacity as a function of $t^{1/2}$. Two separate parts were obtained from this plot before the equilibrium stage was reached (the plateau part): film diffusion (first stage, dotted line) and intraparticle diffusion (second stage, solid line). The resulting straight lines do not pass through the origin for Zn(II); however the value of intercept (β) ranges from −0.52 to +1.25 for temperatures 20−60 °C. This suggests that the boundary layer effect is negligible as the line representing the second part (intraparticle diffusion) is almost crossing the origin. Thus, intraparticle diffusion could be considered as a rate-limiting step during the adsorption of Zn(II). The straight lines do not pass through the origin for Cu(II), but they are close to the origin as the intercept (β) values range from 2.10 to 2.62, showing that the boundary effect is not significant. Thus, intraparticle diffusion resistance affects the adsorption of Cu(II). The rate constant k_i was shown to increase with increasing temperature. For the Pb(II) adsorption the saturation was reached in a very short time and it was not possible to apply the WB model.

In most cases for earlier studies, the removal of heavy metals on biochar followed the PSO model,[58] which showed that the adsorption of Cu(II) and Zn(II) using hardwood and corn straw biochar follows a PSO model. Similar conclusions were made[59] for Cu(II), Zn(II), Cd(II), and Pb(II) on char made from various manures.[60] The use of pinewood and rice husk biochar for the adsorption of Pb(II) also followed a PSO model. In our study, the PSO is also the highest fit, and it assumes a chemisorption.

Thus, in conclusion, the overall mechanism of adsorption was mainly controlled by chemisorption. The corresponding chemisorption mechanisms are shown using the characterization of the SMCB surface using FTIR before and after adsorption. Surface modification of the biochar after adsorption took place, which included the weakening of the C−O bond, the binding of metal ions by the formation of the M−C complex, and the disappearance of the O−H alcohol bond on the biochar surface. In addition, the CEC study indicated that ion exchange is also plays a minor role during the adsorption. Thus, ion exchange, surface binding and complexation, and a strong cation−π interaction may be involved during the adsorption.[18] This result is in correlation with the most fitting PSO model which assumes a chemisorption process. In contrast, the study of the initial solution pH showed a significant increase in the pH during adsorption due to the mineral part of SMCB leading to precipitation. This indicated that precipitation is also involved during adsorption.

3.5. Thermodynamics Test. The effect of temperature is an important physical parameter that must be studied to investigate its contribution on the change of adsorption capacity and efficiency.[30] The most significant adsorption capacity increase with temperature was observed for Zn (Figure 5). Thus, the adsorption was a temperature-dependent process during which a higher and faster adsorption is observed when the temperature is increased. Thermodynamic parameters were obtained by varying the temperature to 20, 40, and 60 °C using the batch technique. The change in Gibbs free energy indicates the spontaneity and feasibility of the adsorption process. The enthalpy change shows if the process is exothermic or endothermic, while the entropy change can reflect the favorability of the adsorption. The results of these parameters are shown in Table 4. For Zn(II), the $\Delta G°$ value is positive at 20 °C and becomes negative when the temperature is increased. This indicates that at room temperature the adsorption process for Zn(II) is not spontaneous. As the temperature is increased, the adsorption process is facilitated and takes place spontaneously. For Pb(II) and Cu(II), $\Delta G°$ is negative, suggesting spontaneous removal using SMCB. Thus, Pb(II) and Cu(II) ions have a higher affinity to SMCB than Zn(II), which was also

Table 4. Gibbs Free Energy Change for Each Metal Ion at Different Temperatures; Enthalpy and Entropy Changes for Each Metal

metal ion	temp, °C	ΔG, kJ/mol	ΔH, kJ/mol	ΔS, kJ/mol
Zn(II)	20	3.73	82.3	0.27
	40	−3.25		
	60	−6.92		
Cu(II)	20	−4.20	125	0.44
	40	−9.98		
	60	−21.95		
Pb(II)	20	−10.39	12.8	0.08
	40	−12.31		
	60	−13.55		

DOI: 10.1021/acs.iecr.9b00749
Ind. Eng. Chem. Res. 2019, 58, 7296−7307

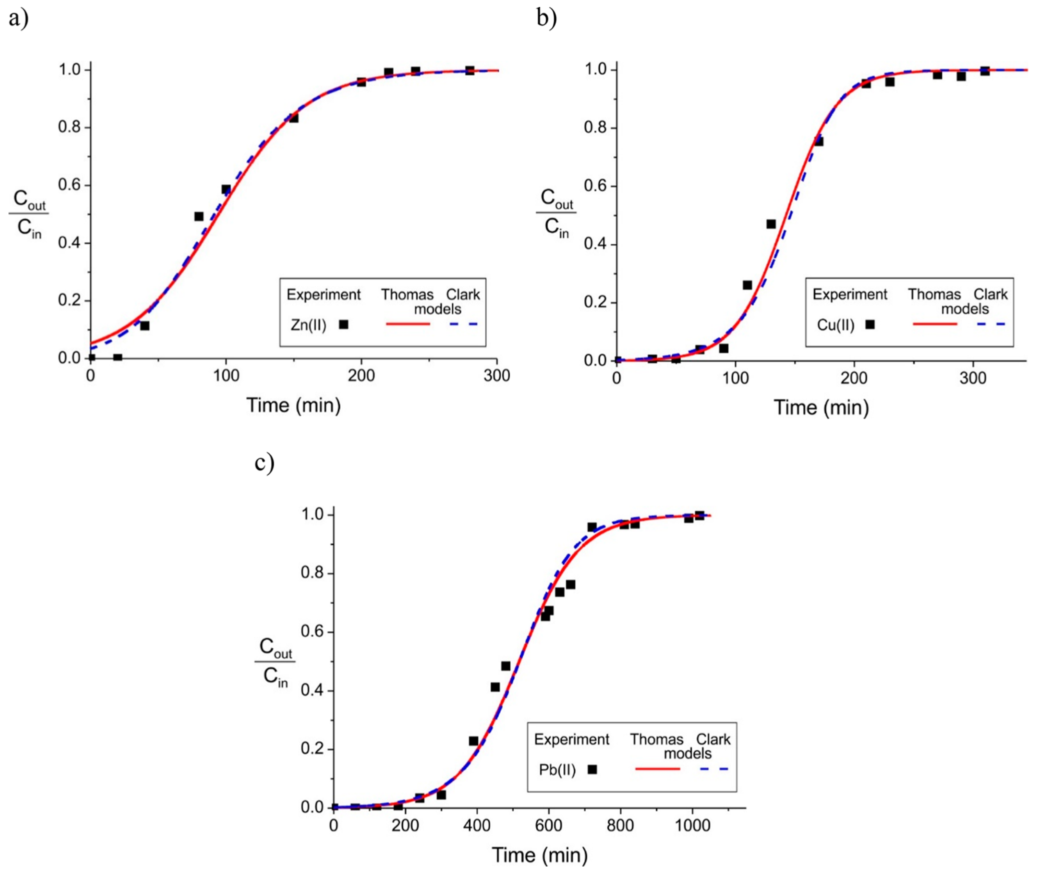

Figure 7. Breakthrough curves of in a single-metal system. (a) Zn, (b) Cu, and (c) Pb ions, described by the Thomas and Clark models in a fixed-bed continuous adsorption.

Table 5. Thomas and Clark Model Parameters for Fixed-Bed Continuous Column

	Thomas model			Clark model		
metal ion	k_{Th}, 10^{-4} mL/min mg	q_{max}, 10^4 mg/g	R^2	A	r, min^{-1}	R^2
Zn(II)	2.55	0.60	0.983	6.379	0.028	0.989
Cu(II)	3.19	1.11	0.991	6709	0.056	0.981
Pb(II)	0.26	12.7	0.985	2331	0.014	0.976

shown by a higher adsorption capacity (Table 3). In addition, the positive values of $\Delta H°$ and $\Delta S°$ prove that the adsorption process was endothermic and favorable with a good affinity between the metals and SMCB.

3.6. Fixed-Bed Column Adsorption Modeling. The breakthrough curve was obtained for the different influent solutions used. It shows that the concentration of metals in the effluent increased with time. Adsorption models are applied to the experimental data to assess the column adsorption parameters, as shown in Figure 7a−c. The parameters obtained are shown in Table 5. The Thomas model was used to determine the kinetic constant k_{Th} and the maximum concentration in the solid phase q_{max}. It assumes that the Langmuir model and pseudo-second order are applied. This assumption was confirmed by the previous kinetics and equilibrium experiments obtained by the batch experiments. The results show that the highest q_{max} value was observed for Pb(II), which confirms the results obtained in the batch experiments as Pb(II) had the highest adsorption capacity. In addition, the Clark model was used, and it assumes that the adsorption process follows the Freundlich isotherm with a neglected axial dispersion in the column. Results show a high correlation factor for both models. From the breakthrough curves, the experimental data and the predicted values from the models show a negligible difference.

From the batch and continuous studies, as well as the characterization of SMCB before and after adsorption, the mechanisms involved during adsorption can be assessed. The characterization of the biochar showed a moderate CEC and chemical interactions on the surface. The study of initial pH implied that precipitation is involved during the sorption process. In contrast, the highest fitting models obtained in the batch kinetic and isotherm studies are in correlation to the Thomas model used for the continuous column adsorption. Therefore, SMCB are potential material that could be used in fixed-bed continuous column for large scale wastewater treatment.

3.7. Competitive Adsorption: Batch and Continuous Systems. Often a competitive adsorption between the metals ions present in wastewater occurs. Thus, it is highly important to study the adsorption process of a multicomponent system of heavy metals. In this study, the coexistence of the three heavy metals was studied in both batch and continuous systems. In the batch experiments, the effect of the mutual presence of Pb^{2+}, Cu^{2+}, and Zn^{2+} was evaluated with varying initial concentration,

DOI: 10.1021/acs.iecr.9b00749
Ind. Eng. Chem. Res. 2019, 58, 7296−7307

as shown in Table 6. The presence of Zn in a single system at a concentration of 1×10^{-3} mol/L showed an adsorption capacity on SMCB of 6.431 mg/g. When adding Pb and Cu (1×10^{-3} mol/L each), the adsorption capacity dropped to 4.238 mg/g. As the concentration of these metals was increased (3×10^{-3} mol/L each), the adsorption capacity became even lower (1.878 mg/g). When the initial concentration of Zn was increased to 3×10^{-3} mol/L and then to 5×10^{-3} mol/L, similar results were observed. The adsorption capacity of Zn at a concentration of 5×10^{-3} mol/L dropped from 20.41 to 2.59 mg/g after addition of 3×10^{-3} mol/L of Cu and Pb. The adsorption capacity of Cu also decreased after the amount of Pb and Zn was increased. However, the decrease was less significant than in the case of Zn, as the adsorption capacity dropped from 6.347 to 6.046 mg/g (initial Cu concentration of 1×10^{-3} mol/L), 19.03 to 15.24 mg/g (initial Cu concentration of 3×10^{-3} mol/L), and 31.65 to 21.70 mg/g (initial Cu concentration of 5×10^{-3} mol/L). As for Pb, the adsorption capacity obtained is significantly higher than that for Cu and Zn in both the single and ternary system, with a negligible decrease in the adsorption capacity when Cu and Zn are added. It was shown to be 20.71, 62.14, and 103.5 mg/g at an initial concentration of 1×10^{-3}, 3×10^{-3}, and 5×10^{-3} mol/L, respectively. Therefore, the results show that the Pb metal ions have the highest affinity to SMCB compared to Cu and Zn during the adsorption process.

Table 6. Adsorption Capacities of the Heavy Metals Ions in a Tertiary Component System

system	q_e (mg/g)		
	Zn(II)	Cu(II)	Pb(II)
Zn (1 mM)	6.431		
Zn (1 mM) + Cu (1 mM) + Pb (1 mM)	4.238	6.291	20.60
Zn (1 mM) + Cu (3 mM) + Pb (3 mM)	1.878	17.86	61.59
Zn (3 mM)	17.80		
Zn (3 mM) + Cu (1 mM) + Pb (1 mM)	7.744	6.226	20.41
Zn (3 mM) + Cu (3 mM) + Pb (3 mM)	5.354	17.55	61.55
Zn (5 mM)	20.41		
Zn (5 mM) + Cu (1 mM) + Pb (1 mM)	5.690	6.164	20.28
Zn (5 mM) + Cu (3 mM) + Pb (3 mM)	2.590	15.81	61.09
Cu (1 mM)		6.347	
Cu (1 mM) + Zn (1 mM) + Pb (1 mM)	5.248	6.264	20.63
Cu (1 mM) + Zn (3 mM) + Pb (3 mM)	7.550	6.046	61.94
Cu (3 mM)		19.03	
Cu (3 mM) + Zn (1 mM) + Pb (1 mM)	3.708	17.58	20.30
Cu (3 mM) + Zn (3 mM) + Pb (3 mM)	4.290	15.24	61.15
Cu (5 mM)		31.65	
Cu (5 mM) + Zn (1 mM) + Pb (1 mM)	2.118	27.09	19.80
Cu (5 mM) + Zn (3 mM) + Pb (3 mM)	2.670	21.70	60.58
Pb (1 mM)			20.71
Pb (1 mM) + Zn (1 mM) + Cu (1 mM)	4.258	6.302	20.58
Pb (1 mM) + Zn (3 mM) + Cu (3 mM)	10.21	18.61	20.51
Pb (3 mM)			62.14
Pb (3 mM) + Zn (1 mM) + Cu (1 mM)	3.728	6.293	62.01
Pb (3 mM) + Zn (3 mM) + Cu (3 mM)	8.260	18.49	61.90
Pb (5 mM)			103.5
Pb (5 mM) + Zn (1 mM) + Cu (1 mM)	2.748	6.280	103.4
Pb (5 mM) + Zn (3 mM) + Cu (3 mM)	5.370	17.49	102.9

Competitive adsorption was also studied in the fixed-bed continuous column to assess the breakthrough curves of the metal cations when present in a single system. The results show that Zn(II) is the first to leave the column in the effluent, followed by Cu(II) and then Pb(II), as shown in Figure 8. Thus, when the metals ions are all present in the column, Zn ions have the least affinity to SMCB, as they do not adsorb as strongly as Cu and Pb ions. These results confirm the earlier conclusion from the batch studies. The breakthrough of the Cu ion takes place shortly after Zn ions, showing that it has a higher affinity than Zn(II), but lower than that of Pb(II). No overshooting of breakthrough is observed, suggesting the same mechanism of adsorption for each ion.

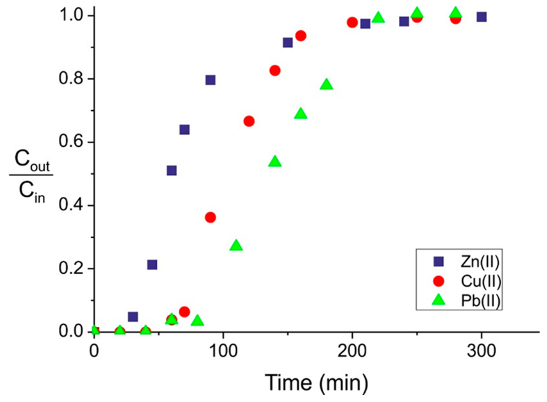

Figure 8. Breakthrough experimental results for Pb, Cu, and Zn ions mutually present in a tertiary system in a fixed-bed continuous adsorption.

4. CONCLUSION

SMCB was used as an adsorbent for the removal of Pb(II), Cu(II), and Zn(II) for wastewater treatment. SMCB was characterized to obtain its physicochemical properties. FTIR studies showed that the functional groups on the surface of the biochar are modified during adsorption. The investigated biochar has a moderate value of cation-exchange capacity. The effect of initial pH was studied, and the pH of the solutions increased at equilibrium. The kinetics test showed that the pseudo-second-order model was the best fit and that intra-particle diffusion plays a role as a rate-limiting step during the adsorption Zn and Cu ions. The best-fitting isotherm model was the Langmuir model. Thermodynamic parameters showed that the adsorption process is endothermic and favorable with good affinity between metals and SMCB. Finally, fixed-bed continuous adsorption was investigated for further application of SMCB in heavy metal adsorption. The breakthrough curve was obtained for each heavy metal modeled by Thomas and Clark expressions. Competitive adsorption was performed in both batch and continuous systems to investigate the adsorption capacity for the mutual presence of the heavy metals. The data show that the highest affinity for SMCB was with the Pb ions followed by Cu and Zn.

■ AUTHOR INFORMATION

Corresponding Author

*E-mail: witold.kwapinski@ul.ie.

ORCID

James J. Leahy: 0000-0001-9642-4526

Witold Kwapinski: 0000-0003-1075-4159

Notes

The authors declare no competing financial interest.

DOI: 10.1021/acs.iecr.9b00749
Ind. Eng. Chem. Res. 2019, 58, 7296−7307

■ ACKNOWLEDGMENTS

The activity was supported by Erasmus+ International Credit Mobility.

■ REFERENCES

(1) Dong, X.; Li, C.; Li, J.; Wang, J.; Liu, S.; Ye, B. A novel approach for soil contamination assessment from heavy metal pollution: A linkage between discharge and adsorption. *J. Hazard. Mater.* **2010**, *175* (1−3), 1022−1030.

(2) Mohan, D.; Pittman, C. U.; Bricka, M.; Smith, F.; Yancey, B.; Mohammad, J.; Steele, P. H.; Alexandre-Franco, M. F.; Gómez-Serrano, V.; Gong, H. Sorption of arsenic, cadmium, and lead by chars produced from fast pyrolysis of wood and bark during bio-oil production. *J. Colloid Interface Sci.* **2007**, *310* (1), 57−73.

(3) Volesky, B.; Holan, Z. R. Biosorption of heavy metals. *Biotechnol. Prog.* **1995**, *11* (3), 235−250.

(4) Kwapinski, W.; Byrne, C. M. P.; Kryachko, E.; Wolfram, P.; Adley, C.; Leahy, J. J.; Novotny, E. H.; Hayes, M. H. B. Biochar from Biomass and Waste. *Waste Biomass Valorization* **2010**, *1* (2), 177−189.

(5) Li, C.; Zhang, L.; Gao, Y.; Li, A. Facile synthesis of nano ZnO/ZnS modified biochar by directly pyrolyzing of zinc contaminated corn stover for Pb(II), Cu(II) and Cr(VI) removals. *Waste Manage.* **2018**, *79*, 625−637.

(6) Dunnigan, L.; Morton, B. J.; Ashman, P. J.; Zhang, X.; Kwong, C. W. Emission characteristics of a pyrolysis-combustion system for the co-production of biochar and bioenergy from agricultural wastes. *Waste Manage.* **2018**, *77*, 59−66.

(7) Nartey, O. D.; Zhao, B. Biochar preparation, characterization, and adsorptive capacity and its effect on bioavailability of contaminants: an overview. *Adv. Mater. Sci. Eng.* **2014**, *2014*, 1−12.

(8) Lehmann, J.; Joseph, S. Earthscan from Routledge. *Biochar for Environmental Management : Science, Technology and Implementation*, 2nd ed.; Routledge, 2015; https://www.routledge.com/Biochar-for-Environmental-Management-Science-Technology-and-Implementation/Lehmann-Joseph/p/book/9780415704151.

(9) Wang, S.; Gao, B.; Zimmerman, A. R.; Li, Y.; Ma, L.; Harris, W. G.; Migliaccio, K. W. Physicochemical and sorptive properties of biochars derived from woody and herbaceous biomass. *Chemosphere* **2015**, *134*, 257−262.

(10) Chen, G.; Peng, C.; Fang, J.; Dong, Y.; Zhu, X.; Cai, H. Biosorption of fluoride from drinking water using spent mushroom compost biochar coated with aluminum hydroxide. *Desalin. Water Treat.* **2016**, *57* (26), 12385−12395.

(11) Gea, F. J.; Santos, M.; Diánez, F.; Tello, J. C.; Navarro, M. J. Effect of spent mushroom compost tea on mycelial growth and yield of button mushroom (Agaricus bisporus). *World J. Microbiol. Biotechnol.* **2012**, *28* (8), 2765−2769.

(12) Jordan, S. N.; Mullen, G. J.; Murphy, M. C. Composition variability of spent mushroom compost in Ireland. *Bioresour. Technol.* **2008**, *99* (2), 411−418.

(13) Chang, K.-L.; Chen, X.-M.; Sun, J.; Liu, J.; Sun, S.; Yang, Z.; Wang, Y. Spent mushroom substrate biochar as a potential amendment in pig manure and rice straw composting processes. *Environ. Technol.* **2017**, *38* (13−14), 1765−1769.

(14) Ye, S.; Zeng, G.; Wu, H.; Zhang, C.; Liang, J.; Dai, J.; Liu, Z.; Xiong, W.; Wan, J.; Xu, P.; Cheng, M. Co-occurrence and interactions of pollutants, and their impacts on soil remediation—A review. *Crit. Rev. Environ. Sci. Technol.* **2017**, *47* (16), 1528−1553.

(15) Ye, S.; Zeng, G.; Wu, H.; Liang, J.; Zhang, C.; Dai, J.; Xiong, W.; Song, B.; Wu, S.; Yu, J. The effects of activated biochar addition on remediation efficiency of co-composting with contaminated wetland soil. *Resour Conserv Recycl.* **2019**, *140*, 278−285.

(16) Karami, N.; Clemente, R.; Moreno-Jiménez, E.; Lepp, N. W.; Beesley, L. Efficiency of green waste compost and biochar soil amendments for reducing lead and copper mobility and uptake to ryegrass. *J. Hazard. Mater.* **2011**, *191* (1−3), 41−48.

(17) Kołodyńska, D.; Krukowska, J.; Thomas, P. Comparison of sorption and desorption studies of heavy metal ions from biochar and commercial active carbon. *Chem. Eng. J.* **2017**, *307*, 353−363.

(18) Ye, S.; Zeng, G.; Wu, H.; Zhang, C.; Dai, J.; Liang, J.; Yu, J.; Ren, X.; Yi, H.; Cheng, M.; Zhang, C. Biological technologies for the remediation of co-contaminated soil. *Crit. Rev. Biotechnol.* **2017**, *37* (8), 1062−1076.

(19) Sun, K.; Jin, J.; Keiluweit, M.; Kleber, M.; Wang, Z.; Pan, Z.; Xing, B. Polar and aliphatic domains regulate sorption of phthalic acid esters (PAEs) to biochars. *Bioresour. Technol.* **2012**, *118*, 120−127.

(20) Ding, Z.; Hu, X.; Wan, Y.; Wang, S.; Gao, B. Removal of lead, copper, cadmium, zinc, and nickel from aqueous solutions by alkali-modified biochar: Batch and column tests. *J. Ind. Eng. Chem.* **2016**, *33*, 239−245.

(21) Han, R.; Wang, Y.; Zhao, X.; Wang, Y.; Xie, F.; Cheng, J.; Tang, M. Adsorption of methylene blue by phoenix tree leaf powder in a fixed-bed column: experiments and prediction of breakthrough curves. *Desalination* **2009**, *245* (1−3), 284−297.

(22) Park, J.-H.; Cho, J.-S.; Ok, Y. S.; Kim, S.-H.; Kang, S.-W.; Choi, I.-W.; Heo, J.-S.; DeLaune, R. D.; Seo, D.-C. Competitive adsorption and selectivity sequence of heavy metals by chicken bone-derived biochar: Batch and column experiment. *J. Environ. Sci. Health, Part A: Toxic/Hazard. Subst. Environ. Eng.* **2015**, *50* (11), 1194−1204.

(23) Schollenberger, C. J.; Simon, R. H. Determination of exchange capacity and exchangeable bases in soil—ammonium acetate method. *Soil Sci.* **1945**, *59* (1), 13−24.

(24) Uzoma, K. C.; Inoue, M.; Andry, H.; Fujimaki, H.; Zahoor, A.; Nishihara, E. Effect of cow manure biochar on maize productivity under sandy soil condition. *Soil Use Manage.* **2011**, *27* (2), 205−212.

(25) Cardenas-Peña, A. M.; Ibanez, J. G.; Vasquez-Medrano, R.; Mexico, D. Determination of the point of zero charge for electrocoagulation precipitates from an iron anode. *Int. J. Electrochem Sci.* **2012**, *7*, 6142−6153.

(26) Desta, M. B. Batch sorption experiments: Langmuir and freundlich isotherm studies for the adsorption of textile metal ions onto teff straw (eragrostis tef) agricultural waste. *J. Thermodyn.* **2013**, *2013* (1), 1−6.

(27) Ho, Y. S.; McKay, G. Kinetic models for the sorption of dye from aqueous solution by wood. *Process Saf. Environ. Prot.* **1998**, *76* (2), 183−191.

(28) Hseu, Z.-Y. Evaluating heavy metal contents in nine composts using four digestion methods. *Bioresour. Technol.* **2004**, *95* (1), 53−59.

(29) Weber, W. J.; Morris, J. C. Kinetics of adsorption on carbon from solution. *J. Sanit Eng. Div.* **1963**, *89* (2), 31−60.

(30) Liu, L.; Lin, Y.; Liu, Y.; Zhu, H.; He, Q. Removal of methylene blue from aqueous solutions by sewage sludge based granular activated carbon: adsorption equilibrium, kinetics, and thermodynamics. *J. Chem. Eng. Data* **2013**, *58* (8), 2248−2253.

(31) Miao, Q.; Bi, E.; Li, B. Roles of polar groups and aromatic structures of biochar in 1-methyl-3-octylimidazolium chloride ionic liquid adsorption: pH effect and thermodynamics study. *Environ. Sci. Pollut. Res.* **2017**, *24* (28), 22265−22274.

(32) Saha, P.; Chowdhury, S. Insight into adsorption thermodynamics.*Thermodynamics*; InTech, 2011; DOI: 10.5772/13474.

(33) Salem, K.; Tsotsas, E.; Mewes, D. Tomographic measurement of breakthrough in a packed bed adsorber. *Chem. Eng. Sci.* **2005**, *60* (2), 517−522.

(34) Thomas, H. C. Heterogeneous ion exchange in a flowing system. *J. Am. Chem. Soc.* **1944**, *66* (10), 1664−1666.

(35) Clark, R. M. Evaluating the cost and performance of field-scale granular activated carbon systems. *Environ. Sci. Technol.* **1987**, *21* (6), 573−580.

(36) Özçimen, D. An approach to the characterization of biochar and bio-oil. *Renew Energy Sustain Futur iConcept Press.* **2013**, 41−58.

(37) Sadaka, S.; Sharara, M.; Ashworth, A.; Keyser, P.; Allen, F.; Wright, A. Characterization of Biochar from Switchgrass Carbonization. *Energies* **2014**, *7* (2), 548−567.

(38) Böke, H.; Akkurt, S.; Özdemir, S.; Göktürk, E. H.; Caner Saltik, E. N. Quantification of CaCO3−CaSO3·0.5H2O−CaSO4·2H2O mix-

tures by FTIR analysis and its ANN model. *Mater. Lett.* **2004**, *58* (5), 723−726.
(39) Viglašová, E.; Galamboš, M.; Danková, Z.; Krivosudský, L.; Lengauer, C. L.; Hood-Nowotny, R.; Soja, G.; Rompel, A.; Matík, M.; Briančin, J. Production, characterization and adsorption studies of bamboo-based biochar/montmorillonite composite for nitrate removal. *Waste Manage.* **2018**, *79*, 385−394.
(40) Samsuri, A. W.; Sadegh-Zadeh, F.; Seh-Bardan, B. J. Characterization of biochars produced from oil palm and rice husks and their adsorption capacities for heavy metals. *Int. J. Environ. Sci. Technol.* **2014**, *11*, 967−976.
(41) Thirumavalavan, M.; Lai, Y.-L.; Lee, J.-F. Fourier Transform Infrared Spectroscopic analysis of fruit peels before and after the adsorption of heavy metal ions from aqueous solution. *J. Chem. Eng. Data* **2011**, *56* (5), 2249−2255.
(42) Lee, J. W.; Kidder, M.; Evans, B. R.; Paik, S.; Buchanan, A. C., III; Garten, C. T.; Brown, R. C. Characterization of Biochars Produced from Cornstovers for Soil Amendment. *Environ. Sci. Technol.* **2010**, *44* (20), 7970−7974.
(43) Subedi, R.; Taupe, N.; Ikoyi, I.; Bertora, C.; Zavattaro, L.; Schmalenberger, A.; Leahy, J. J.; Grignani, C. Chemically and biologically-mediated fertilizing value of manure-derived biochar. *Sci. Total Environ.* **2016**, *550*, 924−933.
(44) Gomez-Eyles, J.; Beesley, L.; Moreno-Jimenez, E.; Ghosh, U.; Sizmur, T. The potential of biochar amendments to remediate contaminated soils. In *Biochar and Soil Biota*; CRC Press, 2013; pp 100−133. DOI: 10.1201/b14585-5.
(45) Domingues, R. R.; Trugilho, P. F.; Silva, C. A.; de Melo, I. C. N. A.; Melo, L. C. A.; Magriotis, Z. M.; Sánchez-Monedero, M. A.; Paz-Ferreiro, J. *PLoS One* **2017**, *12* (5), e0176884.
(46) Lee, J. W.; Buchanan, A. C.; Evans, B. R.; Kidder, M. Oxygenation of biochar for enhanced cation exchange capacity. In *Advanced Biofuels and Bioproducts*; Springer: New York; 2013:35−45. DOI: 10.1007/978-1-4614-3348-4_4.
(47) Franus, M.; Bandura, L. Sorption of heavy metal ions from aqueous solution by glauconite. *Fresenius Environ. Bull.* **2014**, *23* (3), 825−839.
(48) Fiol, N.; Villaescusa, I. Determination of sorbent point zero charge: usefulness in sorption studies. *Environ. Chem. Lett.* **2009**, *7* (1), 79−84.
(49) Simonin, J.-P. On the comparison of pseudo-first order and pseudo-second order rate laws in the modeling of adsorption kinetics. *Chem. Eng. J.* **2016**, *300*, 254−263.
(50) Zhang, S.; Yang, X.; Liu, L.; Ju, M.; Zheng, K. Adsorption behavior of selective recognition functionalized biochar to Cd(II) in wastewater. *Materials* **2018**, *11* (2), 299.
(51) Moradi, O. The Removal of Ions by Functionalized Carbon Nanotube: Equilibrium, Isotherms and Thermodynamic Studies. *Chem. Biochem Eng. Q.* **2011**, *25* (2), 229−240.
(52) Kobya, M.; Demirbas, E.; Senturk, E.; Ince, M. Adsorption of heavy metal ions from aqueous solutions by activated carbon prepared from apricot stone. *Bioresour. Technol.* **2005**, *96* (13), 1518−1521.
(53) Johns, M. M.; Marshall, W. E.; Toles, C. A. Agricultural by-products as granular activated carbons for adsorbing dissolved metals and organics. *J. Chem. Technol. Biotechnol.* **1998**, *71* (2), 131−140.
(54) Bansode, R. R.; Losso, J. N.; Marshall, W. E.; Rao, R. M.; Portier, R. J. Adsorption of metal ions by pecan shell-based granular activated carbons. *Bioresour. Technol.* **2003**, *89* (2), 115−119.
(55) Agouborde, L.; Navia, R. Heavy metals retention capacity of a non-conventional sorbent developed from a mixture of industrial and agricultural wastes. *J. Hazard. Mater.* **2009**, *167* (1−3), 536−544.
(56) Nasernejad, B.; Zadeh, T. E.; Pour, B. B.; Bygi, M. E.; Zamani, A. Camparison for biosorption modeling of heavy metals (Cr (III), Cu (II), Zn (II)) adsorption from wastewater by carrot residues. *Process Biochem.* **2005**, *40* (3−4), 1319−1322.
(57) Park, J. H.; Ok, Y. S.; Kim, S. H.; Cho, J. S.; Heo, J. S.; Delaune, R. D.; Seo, D. C. Evaluation of phosphorus adsorption capacity of sesame straw biochar on aqueous solution: influence of activation methods and pyrolysis temperatures. *Environ. Geochem. Health* **2015**, *37* (6), 969−983.
(58) Chen, X.; Chen, G.; Chen, L.; Chen, Y.; Lehmann, J.; McBride, M. B.; Hay, A. G. Adsorption of copper and zinc by biochars produced from pyrolysis of hardwood and corn straw in aqueous solution. *Bioresour. Technol.* **2011**, *102* (19), 8877−8884.
(59) Kołodyńska, D.; Wnętrzak, R.; Leahy, J. J.; Hayes, M. H. B.; Kwapiński, W.; Hubicki, Z. Kinetic and adsorptive characterization of biochar in metal ions removal. *Chem. Eng. J.* **2012**, *197*, 295−305.
(60) Liu, Z.; Zhang, F.-S. Removal of lead from water using biochars prepared from hydrothermal liquefaction of biomass. *J. Hazard. Mater.* **2009**, *167* (1−3), 933−939.

DOI: 10.1021/acs.iecr.9b00749
Ind. Eng. Chem. Res. 2019, 58, 7296−7307